Brick Strex – A Robust Device Built of LEGO® Bricks for Mechanical Manipulation of Cells

Elina Mäntylä
Tampere University
Teemu Olavi Ihalainen (teemu.ihalainen@tuni.fi)
Tampere University

Research Article

Keywords: normal cell and tissue physiology, cancer, gene expression and signaling

Posted Date: March 31st, 2021

DOI: https://doi.org/10.21203/rs.3.rs-365242/v1

Version of Record: A version of this preprint was published at Scientific Reports on September 16th, 2021.
See the published version at https://doi.org/10.1038/s41598-021-97900-5.

Brick Strex – a robust device built of LEGO® bricks for mechanical manipulation of cells

Elina Mäntylä,[a] Teemu O. Ihalainen[a*]

BioMediTech, Faculty of Medicine and Health Technology, Tampere University, Tampere, Finland[a]

*Address correspondence to Teemu Ihalainen, teemu.ihalainen@tuni.fi

Address: BioMediTech, Faculty of Medicine and Health Technology, Tampere University, Tampere, Finland. Arvo Ylpön katu 34, 33520 Tampere, Finland

Phone: +358 50 3187 202

Abstract

Cellular forces, mechanics and other physical factors are important co-regulators of normal cell and tissue physiology. These cues are often misregulated in diseases such as cancer, where altered tissue mechanics contribute to the disease progression. Furthermore, intercellular tensile and compressive force related signaling is highlighted in collective cell behavior during development. However, the mechanistic understanding on the role of physical forces in regulation of cellular physiology, including gene expression and signaling, is still lacking. This is partly because studies on the molecular mechanisms of force transmission require easily controllable experimental designs. These approaches should enable both easy mechanical manipulation of cells and, importantly, readouts ranging from microscopy imaging to biochemical assays. To achieve a robust solution for mechanical manipulation of cells, we developed devices built of LEGO® bricks allowing cell stretching and compression studies. By using these devices, we show that β-catenin responds differentially to epithelial monolayer stretching and compression, either localizing more to the cell nuclei or cell-cell junctions, respectively. In addition, we show that epithelial compression drives cytoplasmic retention and phosphorylation of transcription coregulator YAP1. We provide a complete part listing and video assembly instructions, allowing other researchers to build and use the devices in cellular mechanics -related studies.

1 Introduction

Cells in our bodies form a complex biochemical and mechanical homeostasis with the surrounding tissues[1,2]. In addition to biochemical signals, cellular physiology is influenced by various physical factors of extracellular environment (topography, rigidity, cell ligand density) and mechanical forces (tensile, shear or compressive forces)[3–7]. Cells can sense physical cues via mechanotransduction process, where mechanical signals are converted into biochemical or electrical activity of the cells. Mechanotransduction events often take place in the cell-extracellular matrix (ECM) and cell-cell adhesions, which both contain mechanosensitive proteins. This allows the cells to transform the mechanical signals into intracellular signaling and adjust the physiological processes accordingly[2,8,9]. Mechanotransduction is achieved when the mechanosensitive proteins respond to mechanical force, expose cryptic binding sites, and trigger downstream signaling cascades such as co-operating Wnt/β-catenin and Hippo pathways or YAP/TAZ signaling[10–18].

In addition to cell-cell and cell-ECM junctions, mechanical forces are also sensed deeper in the cells and they have been shown to directly affect nuclear lamina, chromatin, transcription and genetic programming[16,19–24]. Via these signaling pathways, mechanical forces co-regulate various cellular processes including proliferation, differentiation and cell migration allowing cells to probe the environment and to adjust their physical properties[22,25,26]. Different cell types encounter a variety of mechanical cues: endothelial cells are subjected to shear stress from the blood flow, muscle cells contract and produce strong contractile forces, and epithelial cells experience tension, stretching and compression[27]. Mechanical forces are especially important for normal epithelial homeostasis and they are often altered in diseases such as cancer, where cellular contractility is modified, and higher compressive forces rise from the confined growth of the tumor[28–31]. Furthermore, intercellular contact-induced arrest of cell growth and contact inhibition underlies the homeostatic control of cell growth, density and tissue/organ size[14,32]. In recent years, studies on mechanical stretching have been uncovering the cellular responses to strain[33–36]. However, the opposite phenomenon, lateral compression, has remained understudied despite its importance for e.g., muscle function and implications in cancer.

Studying the effects of mechanical stimuli on cells requires replicable experiments conducted under well controlled *in vitro* conditions with high throughput enabling both microscopy and biochemical analyses. Until now, several approaches have been designed to cover these demands. However, many of the developed devices need special techniques and are most often limited by the small number of cells. In these approaches, single cell or even

subcellular mechanical manipulation is conducted via micromanipulation or by atomic force microscopy[37–39]. However, different and more robust approaches have been developed for larger cell populations. Mechanical compressive stress has been imposed on cells by using different gel- or glass coverslip -based compression schemes[40,41]. Tensile forces have also been imposed to cell populations via different stretching devices, where an elastic cell culture substrate is stretched mechanically or pneumatically[42–46]. Many of these devices function uniaxially, compress a 3D cell culture vertically, or apply biaxial strain[47–55]. Many current market leaders distribute devices with PDMS stretch chambers with actuators for stretch applications including the Nepagene, CellScale and StrexCell[56]. These devices can be excellent for the reproducibility of the experiments but might include downsides. In addition to price, the dynamic range of the movements can be limited, or the size of the devices and the number of cells used do not allow biochemical analyzes preceded by cell fractionation. Here, we describe simple, cost-effective and robust cell stretching devices, Brick Strex S and Brick Strex L, built entirely of LEGO® bricks. These bricks were chosen due to their dimensional precision, low cost, durability and sterilization possibilities. These devices allow uniaxial stretching or compression of large cell populations. The systems can be used manually, or they can be combined with motors of LEGO® Mindstorms®, allowing automation of the stretching experiments. We used the Brick Strex S and L systems for mechanical stimulation of epithelial cells by lateral mechanical compression and thorough immunohistochemical analyses of the cellular responses therein. We envision that the described systems provide an easy starting point for mechanical manipulation of cells and microtissues both in fundamental research and teaching.

In this article, we provide stepwise assembly instructions, parts listing and videos for building the systems. We show that the systems are simple, inexpensive, flexible and applicable with biochemical analyses including immunostaining, cell fractioning, Western blot, and even real-time live-cell confocal microscopy imaging. We present the functionality of our system in studies of mechanobiological phenomena and illustrate that the increased lateral compression of epithelial cells leads to concurrent increase in cell density, reduced cell size, relocalization of β-catenin to the cell vertexes including cell-cell junctions and increased cytoplasmic localization and phosphorylation of transcriptional regulator yes-associated protein 1 (YAP1). Thus, here introduced the Brick Strex systems are a cost-effective and versatile cell manipulation system with high reproducibility enabling mechanical manipulation of the cells with broad implications on the fields of tissue homeostasis and disease pathogenesis.

2 Results

2.1 Construction of Brick Strex S and Brick Strex L devices

The smaller Brick Strex S device is built of only 34 parts (or 24 parts if only one axis is used) to create a robust core, membrane clamps and two axes for tuning the stretch (Figure 1a, Supplementary Table 1 and Supplementary Figure 1). The device is ~5 cm wide, ~8 cm long and ~1.5 cm high enabling easy handling and maintenance in cell culture incubator on a 10 cm Petri dish. After building the core, a Si-membrane (6 x 8 cm) is attached to the bottom of the device by clamping ensuring that the membrane is kept in place even in high stretches. Next, the device is supplemented with a cell culture column cut from a PET-insert and attached to the membrane with silicone grease followed by protein e.g., fibronectin, coating to adapt for cell culture. For a comfortable and easy start, we provide a list of parts and complete assembly figures and videos (Supplementary Table 1, Supplementary Figure 1 and Supplementary Movie 1).

Brick Strex S allows robust stretching experiments with relatively small cell population. In order to increase the substrate surface area to facilitate higher cell numbers and allow live cell imaging we developed larger Brick Strex L device. It contains a 56 -part core (containing membrane clamps and a big worm-geared axel for tuning the stretch) which is combined with a base suitable for live cell imaging in medium (31 bricks) and a lid to cover for protection if desired (20 bricks) (Figure 1b and 1c). The device is ~11 cm wide, ~ 13 cm long and ~ 3 cm high enabling convenient handling and maintenance in cell culture incubator. After building the core, a Si-membrane (6 x 8 cm) is attached by clamping to the bottom of the device and supplemented with a 8.8 cm^2 cell culture column cut from a 50 mL NUNC-tube and attached with silicone grease (optionally, an in-house-3D-printed column can be used, data not shown) followed by fibronectin coating and cell culture as described above. As for the Brick Strex S device, we provide a complete list of parts and assembly instructions and videos for the Brick Strex L (Supplementary Table 2, Supplementary Figure 2-4, Supplementary Movie 2.) Thus, due to the minimalistic and simple design, both of the devices are low-cost, cost-effective and easy to use without any special expertise or maintenance.

2.2 Intracellular localization of β-catenin and YAP in response to increased lateral stretching or compression with Brick Strex S

After constructing the device, we carried out lateral stretching/compression experiments with MDCK type II epithelial cells and Brick Strex S. Here, we analyzed for the cellular mechanical

responses by determining the intracellular localization of β-catenin and/or YAP1. The Wnt/β-catenin pathway and subcellular localization of β-catenin and YAP1 are known to be affected by the cell density, extracellular environment stiffness and modulation of the intercellular junctions[18,57–60]. In a confluent epithelium, β-catenin localizes to the adherence junctions at the plasma membrane via association to E-cadherin[61–64]. In addition, when the Wnt pathway is turned off, β-catenin is constantly being recruited to the "destruction complex" and degraded by proteosomal degradation preventing β-catenin nuclear targeting[63]. Activation of the Wnt pathway results in inhibition of β-catenin breakdown allowing its accumulation, nucleus entry, and finally β-catenin-mediated activation of Wnt target genes[63,65]. Moreover, mechanical strain has also been shown to lead into sequential nuclear accumulation of β-catenin[33]. Respectively, a dense growth condition increases Hippo pathway regulator YAP1 phosphorylation especially from serine 127 (S127) driving YAP1 sequestration, proteasomal degradation and/or retention in the cytoplasm[33,63,65,66]. In contrast, in sparse growth density, loss of contact inhibition and promotion of cellular proliferation, YAP1 is mostly unphosphorylated and predominantly located in the nucleus[61–64]. In addition, increased mechanical strain has been shown to drive YAP1 nuclear localization[67].

In our stretching experiments, the silicon (Si) membrane was first coated with fibronectin and cells ($2x10^4$ cells) were seeded on top (Figure 2a). On the following day, the epithelium was stretched by manually turning the device axes for ¼ of a turn (equal to approx. +7.5% increase in strain) four times with 10-minute intervals. The cells were let to respond to the stretch for 2 h and fixed. In order to investigate the localization of β-catenin in the mechanically stretched epithelium, we stained our samples against β-catenin and F-actin (phalloidin) (n=2). We found that in non-stretched control epithelium, β-catenin was predominantly cytoplasmic with slight accumulation on cell vertexes. In contrast, stretching with the Brick Strex S induced nuclear localization of β-catenin (Figure 2b). This is in line with previous studies on β-catenin -mediated activation of growth and proliferation in the epithelium[33].

Next, we wanted to study the effects of uniaxial lateral compression (Figure 2c) on the mechanotransduction signaling within the epithelium. This was achieved by seeding $2x10^4$ cells into a cell culture column attached to a fibronectin coated Si-membrane pre-stretched into a 25 % strain on Brick Strex S with double axels. Concurrently, cells were equally grown on an unstretched membrane as a control. Cells were grown until a desired confluency (approx. 100 %) was reached and the cells were in physical contact with each other. The compression

experiment was done sequentially by turning the axels ¼ of a turn (equal to approx. 6 % strain relief) in 10-minute intervals until full relaxation was achieved. Cells were kept in the incubator during the recovery between the relaxation sequences. Cells survived the careful and slow manipulation of the membrane and remained attached to the surface. No significant cell death was observed. Finally, the compressed and control cells were fixed at 2 h post substrate manipulation and immunostained against YAP1, or β-catenin and F-actin (phalloidin) (Figure 2). We speculated that as opposite to stretching, the lateral compression would lead into an increase in cell density and growth-inhibitory mechanical signaling. In the compression experiment (Figure 2c) the relief of the 25 % strain led to a ~1.8-fold increase in the cell density compared to that of the non-treated control as depicted by the actin staining (Figure 2d) and the number of DAPI-stained nuclei per growth area (nuclei/mm^2) (Figure 2c, n=3). In the uncompressed less dense control epithelium, YAP1 was mostly nuclear, while in the compressed epithelium with a forced higher cell density, YAP1 was mainly cytoplasmic (Figure 2e). Consequently, in the non-compressed epithelium, β-catenin was mainly located in the cytoplasm and to some extent on the plasma membrane. We did not detect β-catenin in the nucleus. In contrast, in the compressed monolayer β-catenin was less pronounced in the cytoplasm but significantly accumulated into the cell-cell junctions (Figure 2f and 2g, n=2). Together, these results show for the first time that increased intercellular compression leads to cytoplasmic retention of YAP1 and decreased cytoplasmic presence and concerted relocalization of β-catenin to the plasma membrane.

2.3 Biochemical analyses of YAP1 and β-catenin under increased intercellular compression with Brick Strex L

Immunostainings of the compressed epithelium suggested that YAP1 becomes cytoplasmic and that β-catenin becomes less pronounced within the cytoplasm and relocalizes to the cell-cell contacts in response to increased lateral compression. It is acknowledged that in full confluency and in the absence of growth-promoting signaling such as Hippo and Wnt, YAP1 is phosphorylated from serine 127 (S127) enhancing its cytoplasmic retention and degradation, and the cytoplasmic pool of β-catenin is constantly cleaved and degraded[68]. Via these aforementioned mechanisms, both YAP1 and β-catenin are excluded from the nucleus preventing their role as a transcriptional activator. The membrane-association of β-catenin with E-cadherin has been suggested to require ubiquitination and inhibition of proteolytic cleavage leading to its stabilization and accumulation of heavy multi-ubiquitinated forms[6,69]. We

postulated whether the compressive mechanical stress could enforce negative signaling of growth and proliferation. To test our hypothesis and to detect for the phosphorylation of YAP1 and the cytoplasmic presence of YAP1 and β-catenin, biochemical analysis was required. To this end, the cells were grown on non-stretched and stretched (25% strain) fibronectin-coated Si-membranes on the Brick Strex L (n=2) enabling larger amounts of cells to be grown for the biochemical analyses (n=2). After two days of growth and acquiring of confluent growth conditions, the relaxation of the membrane i.e., compression of the cells was accomplished. After a 2 h recovery, the cells were washed and lysed for western blot.

First, the expression and phosphorylation status of the transcription regulator YAP1 of the Hippo-pathway were studied. The analysis showed that in comparison to the untreated control, compression led to the presence of low molecular weight cleavage products of YAP1 suggesting for its proteolytic degradation or cleavage (Figure 3a). In addition, YAP1 S127 phosphorylation levels remained nearly unaltered after the compression in comparison to that in the uncompressed confluent control epithelium (Figure 3b). Together, these results suggest for enforced retention and degradation of YAP1 in the cytoplasm in response to increased lateral compression.

Next, the expression and mobility shift of β-catenin were determined. The experiment showed that in the uncompressed confluent epithelium, the concentration of full length β-catenin was low while low molecular weight fraction was apparently indicative of constant β-catenin degradation within the cytoplasm. In contrast, the compression led to an increase in the presence of the full-length β-catenin and in the emergence of higher molecular weight forms. This suggests for increased accumulation of post-translationally modified forms of β-catenin, inhibition of proteolytic degradation, and stabilization of the protein referring to inhibitory growth signaling. The results are in line with earlier studies showing that membrane-association of β-catenin is preceded by increased post-translational modification and inhibition of its cleavage[67]. However, the low molecular weight fraction was detected both in compressed and uncompressed control samples (Figure 3a). Our immunostaining experiments (Fig. 2g) together with the western blot studies enforce the view that the lateral mechanical compression induces localization of the β-catenin at the cell-cell junctions and inhibition of β-catenin -mediated growth signaling.

2.4 Live-cell imaging of lateral compression -induced cellular packing with Brick Strex L

Brick Strex S and Brick Strex L allowed mechanotransduction studies of adherent cells by using immunofluorescence labeling and western blot. Following these experiments, we wanted to investigate the possibility to use Brick Strex L in live cell imaging. Here we used MDCK cell line stably expressing lamin A chromobody, a nuclear lamina marker. The cells were seeded on pre-stretched membrane and cultured until full confluency (n=2). The imaging was conducted by using an upright fluorescence microscope, allowing high resolution imaging of cells in the device. The device was mounted on the sample stage of an inverted microscope and the 25 % pre-strain was manually relaxed in approximately -1% increments and imaged in between the relaxation steps. Before the imaging, the stage was moved and refocused, allowing the imaging of the same field of view throughout the relaxation. The imaging data was then cropped and aligned (Figure 4a). The analysis showed that the relaxation led to lateral compression of the lamin A chromobody -expressing cells and increased nuclear packing (Figure 4b).

2.5 Cyclic mechanical manipulation of cells using motorized Brick Strex L

To allow studies of cellular mechanotransduction dynamics resembling mechanical conditions within a contracting tissue, cyclic mechanical manipulation is a necessity. For this, we applied a commercially available LEGO® EV3 Intelligent Brick and motor (M size), which has high-working precision, and easy programming by using LEGO® Mindstorms software. This allows automation of the stretching experiments and cyclic manipulation. We used the built-in rotation and color sensors of the EV3 system to achieve an easily programmable cyclic manipulation scheme to match the experimental needs and to drive the manipulation with a mobile phone, tablet or a laptop (Supplementary Figure 5 and 6). The color sensor was used to define the endpoint of the movement and built-in rotation counter was then used to achieve constant strain of the device (Figure 4c). First, we characterized the Brick Strex L performance with the motor. The maximal strain was 31.4% and this strain value was used in following measurements of stretching-relaxation cycle duration and velocity. At highest 100/100 speed of the motor, the cycle took 19.5s which corresponds to 3.2 % strain/s velocity and at lowest motor speed setting of 5/100, the cycle took 316.1s, corresponding to 0.2 % strain/s velocity (Figure 4c). Next, we cultured MDCK cells expressing histone H2B-mCherry on the Brick Strex L to enable visualization of the nuclei in real time during the manipulation. The cells were cultured until

full confluency on pre-strained coated Si-membrane. The motor system allowed a robust control of the experiment: we performed eight (8) stretch–relaxation cycles and imaged the same field between the cycles (Figure 4d, n=2). The imaging was conducted with an upright spinning disk confocal microscope. We noticed a small xy-drift in the imaged field between the cycles, but the drift was easily corrected by manually moving the microscope stage accordingly. Furthermore, the imaging focal plane remained surprisingly stable throughout the experiment. The cyclic manipulation led into a more closely packed epithelial nuclei (Figure 4e), but now the effect was less pronounced when compared to single slow relaxation of pre-strained membrane (Figure 4b).

Taken together, here developed Brick Strex S and Brick Strex L devices allow versatile and multiplexed cell stretching or compression experiments. Our proof-of-principle experiments show that the manipulation can be easily combined with immunofluorescence imaging, biochemical readouts or even live-cell microscopy. By using the devices, we were able to show how stretching or lateral compression of epithelial monolayers influence β-catenin and YAP1 related mechanosignaling.

3 Discussion

Tissues encounter both intrinsic and extrinsic mechanical forces that can influence cellular functions and behavior[70]. The force-related cellular responses have remained understudied partially due to lack of proper tools allowing easy mechanical manipulation of cells and tissues. Furthermore, challenges emerge also from the complexity of the cellular viscoelastic properties, and their variance in accordance with the applied strains, force loading rates and timescales[21]. Moreover, many types of cells work in concert and the interpretation of the results can be difficult due to the collectivity of the cells e.g. in the epithelium[71]. Finally, during the recent years it has become evident that in addition to cell membrane associated adhesion sites, forces can be sensed also deeper in the cells[39,72–74]. Mechanical forces rising from the ECM can be transmitted into the cells and they have been shown to directly affect even cell nuclei and chromatin[75]. Therefore, the tools used in the mechanobiological research should facilitate the use of advanced microscopy methods, biochemical assays, next-generation sequencing and other -omics tools, allowing direct investigation of the force induced effects in signaling pathways, chromatin and other nuclear structures.

In the last two decades, various approaches have been developed to study especially the effect of mechanical stretching on cells and tissues. This has been achieved by constructing

either mechanically or pneumatically actuating devices[76]. In addition, few commercial solutions are also available (e.g., Flexell®, CellScale). These approaches offer precise and highly reproducible ways to conduct cell stretching experiments but often require deep expertise in engineering and manufacturing processes, not necessarily available in every institute. More recently, Boulter et al. constructed a motorized stretching device from homemade elastic silicon elastomer vessel and LEGO® blocks, lowering the manufacturing threshold of such devices[77]. In line with this, we focused on developing a simple, robust, reproducible, well controllable, easily approachable and reconfigurable platform to study how uniaxial stretching or compression affects cells. The platform presented here, Brick Strex, compromises of stretching devices built of LEGO® bricks. The devices are easy to assemble and we provide detailed instructions on how they are constructed. They can be operated manually, or the larger device can also be motorized by the LEGO® EV3 motors and controllers. In addition to the bricks, the system needs only commercially available silicon membrane, thus additional construction steps or parts are not necessary. Thus, they provide a low threshold approach for mechanical manipulation of cells and we envision that they can be easily used also for educational purposes. By using the Brick Strex devices, we show that increased uniaxial inter-cellular i.e., lateral compression results in modulation of YAP1 and β-catenin signaling.

To prove the suitability of the Brick Strex in mechanobiological studies, we first applied lateral stretching to the cells and detected for intracellular localization of β-catenin. In the epithelium, β-catenin is located either in the intercellular junctions as plasma membrane -bound, as cytoplasmic and/or as nucleoplasmic fractions[33]. Once membrane-bound, β-catenin has important adhesion functions, whereas in the nucleus it serves in activation of transcription in the Wnt growth factor signaling pathway[63,65]. Stretching of epithelium has been shown to lead into release of β-catenin from E-cadherin and its nuclear accumulation[33,65,66,78]. This was also evident in our stretching experiment with Brick Strex S and immunostaining of β-catenin. Thus, these experiments indicate that the concept can be used in mechanobiological research and it provides similar cellular responses as previously published devices.

Next, our main aim was to analyze the mechanical responses to increased lateral forces and performed compressions with the Brick Strex device. For this, we detected for the intracellular localization of YAP1 and β-catenin – known mechanosensitive co-regulators of cellular plasticity. Here, our Brick Strex -induced compression experiments pointed to the direction of negative growth signaling: our immunostainings showed that the lateral

compression led to uniaxial contraction of the cell monolayer that induced high cell density, cytoplasmic retention of YAP1 and triggered relocalization of β-catenin to the cell membrane. The acquired data from the biochemical analyses further indicated that compression induced cleavage of YAP1 but did not affect YAP1 phosphorylation at S127P. Cytoplasmic retention of YAP is associated with suppression of nuclear YAP activity and increased contact inhibition and Hippo signaling[32,63]. Importantly, compression promoted the expression of full-length β-catenin together with higher molecular weight fractions suggestive of β-catenin membrane-association and inhibition of β-catenin -mediated growth signaling. Indeed, earlier studies have reported the presence of high molecular weight bands in the membrane-containing cell lysate fractions[79]. Moreover, the high molecular weight β-catenin have been shown to be associated with increased post-translational modifications, namely ubiquitinylation, suggested to be a prerequisite for E-cadherin tethering, and inhibited proteolytic cleavage[67]. In addition, inhibition of Wnt/β-catenin signaling by ubiquitinylation has been shown to be YAP-dependent in cancer[80]. Along these lines, our western blot analyses suggest for increased β-catenin membrane-association in response to lateral compression. Recent advances on cell-cell junction mechanics have indicated that mechanical forces sensed at the junctions lead to distinct mechanical responses at the junctions[39]. Thus, it can be hypothesized that the compression-induced membrane tethering of β-catenin is related in enforcement of the intercellular junctions upon increased mechanical loading. To conclude, by using the Brick Strex mechanical manipulation devices we were able to show that increased lateral compressive forces induce cytoplasmic retention of phosphorylated YAP1. Importantly, we report for the first time that increased uniaxial lateral compression leads to increased membrane-association of β-catenin promoting contact inhibition driving negative regulation of the growth and proliferation of the confluent epithelium.

Finally, we applied our device in live cell microscopy to detect dynamic mechanical changes in the epithelial monolayer. To this end, cells grown to equal confluency on pre-stretched membranes were exposed to compression once or in a cyclic manner, latter of which was accomplished by connecting the device to LEGO® EV3 Intelligent Brick motor. In earlier reports, cyclic mechanical manipulations have led to a strain avoidance response, where cells reorient and change their position away from the direction of the applied strain[81]. Here, cyclic and motorized experiments indicated that once-applied mechanical compression is enough to induce immediate packing of the monolayer at least with large compression strains. In addition to cellular packing, cyclic strain-compression -cycles promote also reorientation of the

epithelial cell nuclei within the monolayer supporting earlier observations. These experiments suggest that this kind of cellular behavior could be dependent on the straining parameters (loading rate, duration, etc.).

To conclude, the Brick Strex devices are well suited to the biochemical analyses of the cells. With these easy and robust devices, we studied the effects of mechanical force on cells using lateral uniaxial lateral compression and immunohistochemical analyses. The experiments presented here prove that the device can be used to trigger mechanotransduction in the epithelium promoting reproducibility and consistency in quantitative mechanobiological studies without costly equipment. As a result, we obtained both fixed and live cell imaging microscopy data on the compressed cells, and finally biochemical analysis data on the modulation of the mechanotransduction signaling without special technical expertise. The application of cost-effective in-house built devices to study epithelial force transduction has a great application value from the methodology perspective. With this being said, the Brick Strex devices with larger sample sizes allow also different genetic analyses of mechanically stretched or compressed cell. In addition, the devices have a wide reach and potential utilization value in the scientific community including teaching and related pedagogical actions. All in all, the presented mechanical manipulation devices with the aforementioned methodological improvements will enable us to understand better the pathophysiology and important processes of mechanotransduction.

4 Materials and methods

4.1 Cell culture

Madin-Darby canine kidney (MDCK) type II cells were maintained in low glucose MEM (#51200046, Thermo Fisher Scientific, Waltham, MA, USA) supplemented with 1 % (vol/vol) penicillin-streptomycin antibiotics (#15140122, Thermo Fisher Scientific) and 10 % fetal bovine serum (#10500064, Thermo Fisher Scientific) under standard conditions in a humidified cell incubator (+37 °C, 5 % CO_2). For the lateral compression experiments, 2 x 10^4 cells for microscopy imaging (Brick Strex S) or 8 x10^4 cells for biochemical assays (Brick Strex L) were seeded in cell culture columns attached onto fibronectin (10 µg/mL) coated and UV-treated (30 min) thin (0.01") USP class VI silicone (Si) membranes (8x4.5 cm, Specialty Manufacturing, Inc., Saginaw, MI, USA) using high-vacuum silicone grease (Dow Corning®, Merck, Darmstadt, Germany). The Si-membranes were assembled in Brick Strex with 25 % strain (measured as 25 % increase in stretch). The columns were prepared by cutting the column

off from a PET insert (small device) or by using 8.8 cm^2 plastic ring with a height of 1 cm (Brick Strex L). As a control, cells were seeded also on unstretched Si-membranes in similar columns. Cells were grown until a suitable confluency was reached.

4.2 Immunolabelling

Immunostaining of the samples was done within the attached cell culture columns. Cell samples were fixed with MetOH (ice cold, 5 min, RT), washed twice with PBS and incubated directly with a primary rabbit antibody against β-catenin (1:2000 in 3 % BSA-PBS, ab6302, Abcam, Cambridge, UK), or fixed with 4 % paraformaldehyde (10 min, RT), washed twice with PBS, permeabilized with 0.5 % Triton-X100 - 0.5 % BSA in PBS (á 10 min, RT) and treated with a mouse monoclonal antibody against YAP1 (1:500 in 3 % BSA-PBS, YAP163.7, sc-101199, Santa Cruz Biotechnology, Dallas, USA) and Alexa565-conjugated phalloidin to detect actin (1:100 in 3 % BSA-PBS, 1 h in RT, in dark). After the primary antibody incubation, the samples were washed with permeabilization buffer (0.5 % Triton-X100 - 0.5 % BSA in PBS), PBS and again with permeabilization buffer (á 10 min, RT). Next, Alexa 488-conjugated goat anti-mouse and Alexa 647-conjugated goat anti-rabbit secondary antibodies (Thermo Fisher Scientific, Waltham, MA, USA) were added and incubated for 1h (1:200 in 3 % BSA-PBS, RT, in dark). After the secondary antibody incubation, the samples were washed twice with PBS (á 10 min, RT, in dark) and rinsed once with dH_2O. The samples were detached from the stretching device and the column was detached followed by removal of the silicon grease. Finally, 18 x 18 nm silicon piece was cut out and moved to an objective glass and mounted with ProLong Diamond Antifade Mountant with DAPI (Thermo Fisher Scientific) by placing a 22x22 high-performance glass coverslip (Carl Zeiss Microscopy) on top. Samples were cured in RT in dark o/n and stored in +4°C prior to imaging.

4.3 Microscopy

Confocal microscopy of the samples was conducted using Nikon A1R laser scanning confocal microscope mounted in inverted Nikon Ti–E (Nikon Instruments Europe BV, Amsterdam, Netherlands). The excitation laser lines and emission filters were 405 nm and BP450/50 nm; 488 nm and 525/50; 561 nm and BP595/50 nm; and 633 nm and 700/75 nm. The laser intensity was adjusted to minimize photobleaching. The images were collected using a Plan-Apochromat 60x/1.4 oil immersion objective. The detector sensitivity was adjusted for each sample to optimize the image brightness and to avoid saturation. The data was collected as images of size

1024 × 1024 pixels with a pixel size of 83 nm in x/y, and as 3D z-stacks containing 80-100 slices with 200 nm intervals.

For live cell imaging during manual relaxation, MDCK cells expressing Lamin A-EGFP-chromobody were cultured on fibronectin (10 µg/mL) coated thin Si membrane assembled in Brick Strex L with a 25 % pre-strain and enclosed into a base with a brick lid. Once the desired confluency was reached, the device was attached with metal clamps onto a pre-heated Nikon Eclipse FN1 upright microscope stage. For imaging, CoolLED pE-4000 was used as a light source (470nm LED) to image using a pre-heated water dip objective (Nikon CFI Apo LWD 25x/1.1, WD 2.0 mm). Images of were acquired with Hamamatsu Orca-Flash4.0 V2 CMOS camera.

Live cell imaging of cyclic stretching using MDCK cells expressing histone H2B-mCherry fusion protein was conducted with X-Light V2 spinning-disk confocal system (CrestOptics S.p.A., Rome, Italy) mounted in the above-mentioned Nikon FN1 upright microscope. Water dip objective (Nikon CFI Apo LWD 25x/1.1, WD 2.0 mm) was used together with 470nm LED excitation from Spectra X (Lumencor, Beaverton, OR, USA) and 540/50 emission filter. Andor iXon Life 888 camera (Andor, Belfast, UK) was used to acquire the image.

4.4 Cell lysis and western blot

For western blotting, the cells were seeded in 8.8 cm^2 cell culture column prepared by cutting from 50 mL NUNC-tube and attached with silicone grease on fibronectin (10 µg/mL) coated thin Si membrane assembled in Brick Strex L with a 25 % strain. In control studies, the cells were seeded on unstretched Si-membranes. To detect the mechanosensitive proteins prior and after the relaxation, the cells from the control and the compressed membranes, respectively, were lysed as previously described[82]. To this end, Brick Strex L devices were put on ice and the medium was aspirated followed by rinse with ice-cold PBS. Next, the cells were overlaid with 0.5 mL of cell lysis buffer [100 mM KCl, 5 mM $MgCl_2$, 10 mM Hepes, pH 7.0, 0.5 % NP-40, and 10 000 U/mL Halt™ Protease Inhibitor Cocktail 100X (#78429, Thermo Fisher Scientific)] and detached by scraping on ice. The cell lysate was next transferred into a tube pre-cooled on ice. After incubation for 10 min at +4°C on ice, the samples were centrifuged at 5000 rpm for 5 min followed by collection of the supernatants considered to be the cytoplasmic fractions while the pellets were kept as to obtain the nuclear fraction. The nuclear fraction was produced by resuspending the pellets in 250 µl of cold high salt lysis buffer [400 mM KCl, 5 mM $MgCl_2$, 10 mM Hepes, pH 7.0, 0.5 % NP-40, 1 mM DTT, and 10 000 U/mL protease

inhibitor cocktail]. Next, the tubes were vigorously rocked at +4 °C for 45 min on a shaking platform. The supernatants i.e. the nuclear extracts were collected after centrifugation at 10 000 × *g* for 30 min. The cytoplasmic and nucleic lysates were then pooled to produce a total lysate. Finally, the protein concentrations were measured with NanoDrop and the samples were stored in -70°C prior immunoblotting.

For the western blot, a total of 20 µg of protein was mixed with SDS-Laemmli 4X sample buffer and boiled for 10 min. After cooling, the samples were briefly centrifuged (10 000 × g for 1 min) and loaded on a NuPAGE 4-12 % gradient gel (Invitrogen) along with a prestained dual-color molecular weight marker (#161-0376, Bio-Rad, Hercules, CA, USA). The gel was run for 5 min at 90 V after which the voltage was increased to 180 V to finish the run. Proteins were transferred to a PVDF membrane for 7 min at constant current of 400 mA (Trans-Blot®Turbo™ transfer system with PowerPac Basic power unit, Bio-Rad). After the run, the blot was blocked in 3 % BSA in Tris-buffered saline (1X TBS) for 1h at RT. The blot was then incubated with a primary antibody against YAP1 (1:1000, YAP163.7, sc-101199, Santa Cruz Biotechnology), β-actin (1:5000, ab6276, Abcam), YAP1 S127P (1:1000, #13008, Cell Signaling Technology, Denvers, MA, USA), β-catenin (1:1000, ab6302, Abcam), H3 (1:1000, ab1791, Abcam) or H3K9me3 (1:1000, ab8899, Abcam) for o/n in +4 °C in tilting, rinsed three times with 0.1 % Tween 20-TBS (TBST, á 10 min, RT, in tilting), and incubated with a horseradish peroxidase -conjugated goat-anti mouse/rabbit secondary Abs for 1 h in RT (in tilting). Finally, the blot was washed three times with TBST and once with dH2O (á 10 min, RT, in tilting). The detection was done by applying Pierce™ ECL Western Blotting Substrate (Thermo Fisher Scientific) to the blot following manufacturer´s instructions and imaged using a Bio-Rad´s CCD-camera based ChemiDoc™ XRS+ system (Bio-Rad).

4.5 Device construction and characterization

The Brick Strex devices (Figure 1) were assembled of LEGO® bricks (Supplementary Table 1 and 2, and supplementary Figures 1 – 4) and detailed assembly instructions are provided in the supplements (Supplementary Movie 1 and 2). Brick Strex L device base was sealed to avoid medium leaks with poly(dimethylsiloxane) (PDMS) (1:10 w/w, curing agent: Sylgard 184 pre-polymer, Sigma-Aldrich). For motorization of Brick Strex L device, LEGO® servomotor M was used together with color sensor (Supplementary Figure 5). The motor was controlled with LEGO® EV3 Intelligent Brick. Cyclic stretching was programmed using LEGO® Mindstorms software (Supplementary Figure 6 and Supplementary Movie 3).

For plating the cells, Si membrane was clamped to the device, a cell culture column was attached using silicone grease, and the membrane was coated with fibronectin and treated with UV for 30 min. Next, the excess fibronectin was aspirated, and the membrane was washed once with PBS. Medium (2 mL) was added to the column and the whole device was brought into the cell incubator 15 min prior plating the cells for stabilization of the pH and temperature. To characterize the uniaxial stretch, a 3D printed mold was used to mark the stretched silicone membrane with an array of dots, or by applying fluorescent beads on the stretched membrane (FluoSpheres™ Polystyrene Microspheres, 1.0 μm, yellow/green fluorescent (505/515), Thermo Fisher Scientific) (data not shown). The membrane was then imaged with Nikon AZ100 Multizoom upright fluorescence macroscope with built-in 8X zoom optics using a 5X objective (Nikon AZ-Plan Fluor 5x/0.50, working distance (WD) 15.0 mm, air). Excitation was done by using C-HGFI Precentered Fiber epifluorescence 100 W mercury illuminator as a light source and emission was collected by using 520/35 filter. Image capturing was done with DFK 33UX250 CMOS color camera. The quality of stretch was analyzed by measuring the distance of the drawn points prior and post the relaxation of the membrane with a digital caliper (data not shown).

5 References

1. Humphrey, J. D., Dufresne, E. R. & Schwartz, M. A. Mechanotransduction and extracellular matrix homeostasis. *Nat. Rev. Mol. Cell Biol.* **15**, 802–812 (2014).
2. Iskratsch, T., Wolfenson, H. & Sheetz, M. P. Appreciating force and shape — the rise of mechanotransduction in cell biology. *Nat. Rev. Mol. Cell Biol.* **15**, 825–833 (2014).
3. DuFort, C. C., Paszek, M. J. & Weaver, V. M. Balancing forces: architectural control of mechanotransduction. *Nat. Rev. Mol. Cell Biol.* **12**, 308–319 (2011).
4. Nemec, S. & Kilian, K. A. Materials control of the epigenetics underlying cell plasticity. *Nat. Rev. Materials*. **6**, 69–83 (2021).
5. Kechagia, J. Z., Ivaska, J. & Roca-Cusachs, P. Integrins as biomechanical sensors of the microenvironment. *Nat. Rev. Mol. Cell Biol.* **20**, 457–473 (2019).
6. Romani, P., Valcalcer-Jimenez, L., Frezza, C. & Dupont, S. Crosstalk between mechanotransduction and metabolism. *Nat. Rev. Mol. Cell Biol.* **22**, 22–38 (2021).
7. Nemec, S. & Kilian, K. A. Materials control of the epigenetics underlying cell plasticity. *Nat. Rev. Mat.* **6**, 69–83 (2020).
8. Wang, N., Tytell, J. D. & Ingber, D. E. Mechanotransduction at a distance: Mechanically coupling the extracellular matrix with the nucleus. *Nat. Rev. Mol. Cell Biol.* **10**, 75–82 (2009).
9. Ladoux, B. & Mège, R. M. Mechanobiology of collective cell behaviours. *Nat. Rev. Mol. Cell Biol.* **18**, 743–757 (2017).
10. Lemmon, C. A., Chen, C. S. & Romer, L. H. Cell traction forces direct fibronectin matrix assembly. *Biophys. J.* **96**, 729–738 (2009).
11. Lemmon, C. A. & Weinberg, R. A. Multiple cryptic binding sites are necessary for robust fibronectin assembly: An in silico study. *Sci. Rep.* **7**, 18061, 10.1038/s41598-017-18328-4 (2017).
12. Zhong, C. *et al.* Rho-mediated contractility exposes a cryptic site in fibronectin and induces fibronectin matrix assembly. *J. Cell Biol.* **141**, 539–551 (1998).
13. Du, J. *et al.* Extracellular matrix stiffness dictates Wnt expression through integrin pathway. *Sci. Rep.* **6**, 1–12 (2016).
14. Dietrich, C., Scherwat, J., Faust, D. & Oesch, F. Subcellular localization of β-catenin is regulated by cell density. *Biochem. Biophys. Res. Commun.* **292**, 195–199 (2002).
15. Varelas, X. *et al.* The Hippo pathway regulates Wnt/β-catenin signaling. *Dev. Cell.* **18**, 579–591 (2010).

16. Osmanagic-Myers, S., Dechat, T. & Foisner, R. Lamins at the crossroads of mechanosignaling. *Genes Dev*. **29**, 225–237 (2015).
17. Pan, Y., Heemskerk, I., Ibar, C., Shraiman, B. I. & Irvine, K. D. Differential growth triggers mechanical feedback that elevates Hippo signaling. *Proc. Natl. Acad. Sci. USA.* **113**, E6974–E6983, 10.1073/pnas.1615012113 (2016).
18. Cha, B. *et al.* Mechanotransduction activates canonical Wnt/β-catenin signaling to promote lymphatic vascular patterning and the development of lymphatic and lymphovenous valves. *Genes Dev.* **30**, 1454–1469 (2016).
19. Cho, S., Irianto, J. & Discher, D. E. Mechanosensing by the nucleus: From pathways to scaling relationships. *J. Cell Biol.* **216**, 305–315 (2017).
20. Kaminski, A., Fedorchak, G. R. & Lammerding, J. The cellular mastermind(?)-mechanotransduction and the nucleus. *Prog. Mol. Biol. Transl. Sci.* **126**, 157–203 (2014).
21. Kirby, T. J. & Lammerding, J. Emerging views of the nucleus as a cellular mechanosensor. *Nat. Cell Biol.* **20**, 373–381 (2018).
22. Swift, J. *et al.* Nuclear lamin-A scales with tissue stiffness and enhances matrix-directed differentiation. *Science.* **341**, 1240104, 10.1126/science.1240104 (2013).
23. Iyer, K. V., Pulford, S., Mogilner, A. & Shivashankar, G. V. Mechanical activation of cells induces chromatin remodeling preceding MKL nuclear transport. *Biophys. J.* **103**, 1416–1428 (2012).
24. Miroshnikova, Y. A., Nava, M. M. & Wickström, S. A. Emerging roles of mechanical forces in chromatin regulation. *J. Cell Sci.* **130**, 2243–2250 (2017).
25. He, L., Si, G., Huang, J., Samuel, A. D. T. & Perrimon, N. Mechanical regulation of stem-cell differentiation by the stretch-activated Piezo channel. *Nature.* **555**, 103–106 (2018).
26. van Helvert, S., Storm, C. & Friedl, P. Mechanoreciprocity in cell migration. *Nat. Cell Biol.* **20**, 8–20 (2018).
27. Jaalouk, D. E. & Lammerding, J. Mechanotransduction gone awry. *Nat. Rev. Mol. Cell Biol.* **10**, 63–73 (2009).
28. Butcher, D. T., Alliston, T. & Weaver, V. M. A tense situation: forcing tumour progression. *Nat. Rev. Cancer.* **9**, 108–122 (2009).
29. Nia, H. T. *et al.* Solid stress and elastic energy as measures of tumour mechanopathology. *Nat. Biomed. Eng.* **1**, 0004, 10.1038/s41551-016-0004 (2017).

30. Fernández-Sánchez, M. E. *et al.* Mechanical induction of the tumorigenic β-catenin pathway by tumour growth pressure. *Nature.* **523**, 92–95 (2015).
31. Sharif, G. M. & Wellstein, A. Cell density regulates cancer metastasis via the Hippo pathway. *Future Oncol.* **11**, 3253–6320 (2015).
32. Schnyder, S. K., Molina, J. J. & Yamamoto, R. Control of cell colony growth by contact inhibition. *Sci. Rep.* **10**, 6713, 10.1038/s41598-020-62913-z (2020).
33. Benham-Pyle, B. W., Pruitt, B. L. & Nelson, W. J. Mechanical strain induces E-cadherin-dependent Yap1 and β-catenin activation to drive cell cycle entry. *Science.* **348**, 1024–1027 (2015).
34. Wang, Y. *et al.* Mechanical strain induces phenotypic changes in breast cancer cells and promotes immunosuppression in the tumor microenvironment. *Lab. Invest.* **100**, 1503–1516 (2020).
35. Nava, M. M. *et al.* Heterochromatin-driven nuclear softening protects the genome against mechanical stress-induced damage. *Cell.* **181**, 800-817.e22, 10.1016/j.cell.2020.03.052 (2020).
36. Mohan, A. *et al.* Spatial proliferation of epithelial cells is regulated by E-cadherin force. *Biophys. J.* **115**, 853–864 (2018).
37. Fedorchak, G. & Lammerding, J. Cell microharpooning to study nucleo-cytoskeletal coupling. in *Methods. Mol. Biol.* **1411**, 241–254 (2016).
38. Trache, A., Xie, L., Huang, H., Glinsky, V. V. & Meininger, G. A. Applications of atomic force microscopy for adhesion force measurements in mechanotransduction. in *Methods Mol, Biol.* **1814**, 515–528 (2018).
39. Esfahani, A. M. *et al.* Characterization of the strain-rate–dependent mechanical response of single cell–cell junctions. *Proc. Natl. Acad. Sci.* **118**, e2019347118, 10.1073/pnas.2019347118 (2021).
40. Ihalainen, T. O. *et al.* Differential basal-to-apical accessibility of lamin A/C epitopes in the nuclear lamina regulated by changes in cytoskeletal tension. *Nat. Mat.* **14**, 1252–1261 (2015).
41. Damodaran, K. *et al.* Compressive force induces reversible chromatin condensation and cell geometry–dependent transcriptional response. *Mol. Biol. Cell.* **29**, 3039–3051 (2018).
42. Kreutzer, J. *et al.* Pneumatic cell stretching system for cardiac differentiation and culture. *Med. Engi. Phys.* **36**, 496–501 (2014).

43. Mukundan, V., Nelson, W. J. & Pruitt, B. L. Microactuator device for integrated measurement of epithelium mechanics. *Biomed. Microdevices.* **15**, 117–123 (2013).

44. Schürmann, S. *et al.* The IsoStretcher: An isotropic cell stretch device to study mechanical biosensor pathways in living cells. *Biosens. Bioelectron.* **81**, 363–372 (2016).

45. Dhein, S. *et al.* Mechanical control of cell biology. Effects of cyclic mechanical stretch on cardiomyocyte cellular organization. *Prog. Biophys. Mol.* **115**, 93–102 (2014).

46. Atcha, H. *et al.* A low-cost mechanical stretching device for uniaxial strain of cells: A platform for pedagogy in mechanobiology. *J. Biomech. Eng.* **140**, 81005–81006 (2018).

47. Iwadate, Y. & Yumura, S. Cyclic stretch of the substratum using a shape-memory alloy induces directional migration in Dictyostelium cells. *BioTechniques.* **47**, 757–767 (2009).

48. Huh, D. *et al.* Reconstituting organ-level lung functions on a chip. *Science.* **328**, 1662–1668 (2010).

49. Huang, Y. & Nguyen, N. T. A polymeric cell stretching device for real-time imaging with optical microscopy. *Biomed. Microdevices.* **15**, 1043–1054 (2013).

50. Deguchi, S., Kudo, S., Matsui, T. S., Huang, W. & Sato, M. Piezoelectric actuator-based cell microstretch device with real-time imaging capability. *AIP Advances.* **5**, 067110, 10.1063/1.4922220 (2015).

51. Wyatt, T. P. J. *et al.* Actomyosin controls planarity and folding of epithelia in response to compression. *Nat. Mat.* **19**, 109–117 (2020).

52. Tschumperlin, D. J. *et al.* Bronchial epithelial compression regulates MAP kinase signaling and HB-EGF-like growth factor expression. *Am. J. Physiol. Lung Cell Mol. Physiol.* **282**, L904–L911, 10.1152/ajplung.00270.2001 (2002).

53. Lee, D., Erickson, A., You, T., Dudley, A. T. & Ryu, S. Pneumatic microfluidic cell compression device for high-throughput study of chondrocyte mechanobiology. *Lab Chip.* **18**, 2077–2086 (2018).

54. Heo, Y. J., Kan, T., Iwase, E., Matsumoto, K. & Shimoyama, I. Stretchable cell culture platforms using micropneumatic actuators. *Micro Nano Lett.* **8**, 865–868 (2013).

55. Kamble, H., Vadivelu, R., Barton, M., Shiddiky, M. J. A. & Nguyen, N. T. Pneumatically actuated cell-stretching array platform for engineering cell patterns: In vitro. *Lab Chip.* **18**, 765–774 (2018).

56. StrexCell: Cell Stretching and Freezing | Strex Cell. https://strexcell.com/.

57. van Noort, M., Meeldijk, J., van der Zee, R., Destree, O. & Clevers, H. Wnt signaling controls the phosphorylation status of β-catenin. *J Biol. Chem.* **277**, 17901–17905 (2002).

58. Avvisato, C. L. *et al.* Mechanical force modulates global gene expression and β-catenin signaling in colon cancer cells. *J Cell Sci.* **120**, 2672–2682 (2007).

59. Chen, H. N. *et al.* PDLIM1 stabilizes the E-Cadherin/b-catenin complex to prevent epithelial-mesenchymal transition and metastatic potential of colorectal cancer cells. *Cancer Res.* **76**, 1122–1134 (2016).

60. Charras, G. & Yap, A. S. Tensile forces and mechanotransduction at cell-cell junctions. *Curr. Biol.* **28**, R445–R457, 10.1016/j.cub.2018.02.003 (2018).

61. Kam, Y. & Quaranta, V. Cadherin-bound β-catenin feeds into the Wnt pathway upon adherens junctions dissociation: evidence for an intersection between β-catenin pools. *PLoS One.* **4**, e4580, 10.1371/journal.pone.0004580 (2009).

62. Kim, W. K. *et al.* β-catenin activation down-regulates cell-cell junction-related genes and induces epithelial-to-mesenchymal transition in colorectal cancers. *Sci. Rep.* **9**, 18440, 10.1038/s41598-019-54890-9 (2019).

63. Zhao, B. *et al.* Inactivation of YAP oncoprotein by the Hippo pathway is involved in cell contact inhibition and tissue growth control. *Gen. Dev.* **21**, 2747–2761 (2007).

64. Kafri, P. *et al.* Quantifying β-catenin subcellular dynamics and cyclin D1 mRNA transcription during Wnt signaling in single living cells. *eLife.* **5**, e16748, 10.7554/eLife.16748 (2016).

65. Furukawa, K. T., Yamashita, K., Sakurai, N. & Ohno, S. The epithelial circumferential actin belt regulates YAP/TAZ through nucleocytoplasmic shuttling of Merlin. *Cell Rep.* **20**, 1435–1447 (2017).

66. Driscoll, T. P., Cosgrove, B. D., Heo, S. J., Shurden, Z. E. & Mauck, R. L. Cytoskeletal to nuclear strain transfer regulates YAP signaling in mesenchymal stem cells. *Biophys. J.* **108**, 2783–2793 (2015).

67. Aberle, H., Bauer, A., Stappert, J., Kispert, A. & Kemler, R. β-catenin is a target for the ubiquitin-proteasome pathway. *EMBO J.* **16**, 3797–3804 (1997).

68. Charras, G. & Yap, A. S. Tensile forces and mechanotransduction at cell-cell junctions. *Curr. Biol.* **28**, R445–R457, 10.1016/j.cub.2018.02.003. (2018).

69. Haq, S. *et al.* Stabilization of β-catenin by a Wnt-independent mechanism regulates cardiomyocyte growth. *Proc. Natl. Acad Sci. U.S.A.* **100**, 4610–4615 (2003).

70. Tambe, D. T. *et al.* Collective cell guidance by cooperative intercellular forces. *Nat. Mat.* **10**, 469–475 (2011).

71. Miroshnikova, Y. A., Nava, M. M. & Wickström, S. A. Emerging roles of mechanical forces in chromatin regulation. *J. Cell Sci.* **130**, 2243–2250 (2017).

72. Kamble, H., Barton, M. J., Jun, M., Park, S. & Nguyen, N. T. Cell stretching devices as research tools: engineering and biological considerations. *Lab Chip.* **16**, 3193–3203 (2016).

73. Brosig, M., Ferralli, J., Gelman, L., Chiquet, M. & Chiquet-Ehrismann, R. Interfering with the connection between the nucleus and the cytoskeleton affects nuclear rotation, mechanotransduction and myogenesis. *Int. J. Biochem. Cell Biol.* **42**, 1717–1728 (2010).

74. Kreutzer, J. *et al.* Pneumatic unidirectional cell stretching device for mechanobiological studies of cardiomyocytes. *Biomech Model Mechanobiol.* **19**, 291–303 (2020).

75. Boulter, E., Tissot, F. S., Dilly, J., Pisano, S. & Féral, C. C. Cyclic uniaxial mechanical stretching of cells using a LEGO® parts-based mechanical stretcher system. *J Cell Sci.* **133**, 10.1242/jcs.234666 (2020).

76. Dietrich, C., Scherwat, J., Faust, D. & Oesch, F. Subcellular localization of β-catenin is regulated by cell density. *Biochem. Biophys. Res. Commun.* **292**, 195–199 (2002).

77. Klaus, A. & Birchmeier, W. Wnt signalling and its impact on development and cancer. *Nat. Rev. Cancer* **8**, 387–398 (2008).

78. Benham-Pyle, B. W., Sim, J. Y., Hart, K. C., Pruitt, B. L. & Nelson, W. J. Increasing β-catenin/Wnt3A activity levels drive mechanical strain-induced cell cycle progression through mitosis. *eLife* **5**, e19799, 10.7554/eLife.19799.001 (2016).

79. Goretzky, T. *et al.* Beta-catenin cleavage enhances transcriptional activation. *Sci. Rep.* **8**, 671, 10.1038/s41598-017-18421-8 (2018).

80. Chen, C. *et al.* YAP-dependent ubiquitination and degradation of β-catenin mediates inhibition of Wnt signalling induced by Physalin F in colorectal cancer article. *Cell Death Dis.* **9**, 1–14 (2018).

81. Tamiello, C., Bouten, C. V. C. & Baaijens, F. P. T. Competition between cap and basal actin fiber orientation in cells subjected to contact guidance and cyclic strain. *Sci. Rep.* **5**, 8752, 10.1038/srep08752 (2015).

82. Wang, W. *et al.* Imaging and characterizing influenza A virus mRNA transport in living cells. *Nucleid Acids Res.* **36**, 4913–4928 (2008).

6 Acknowledgements

We are grateful for Jukka Lehtiniemi and Dr. Markus Hannula from Tampere University for taking most of the photos and videos of the stretchers. Oliver Priimägi and Santeri Karttunen are acknowledged for their work in listing of the device parts. We thank Dr. Soile Nymark for the support and comments on the manuscript. This work was supported by the Academy of Finland under the award numbers 308315 and 314106 (TOI) and 332615 (EM). LEGO® is a trademark of the LEGO Group of companies which does not sponsor, authorize or endorse this article.

7 Author contributions

E.M. designed and performed the experiments, wrote the manuscript and prepared the figures. T.O.I. designed the hypotheses, built the prototypes of the Brick Strex devices, wrote the manuscript and prepared figures of the manuscript.

8 Additional information

8.1 Competing interest statement

The authors declare that they have no competing interests.

9 Figure legends

Figure 1. Brick Strex devices and their structure.

Design of the various cell stretching devices built of LEGO® bricks. **a**, Side and top views of Brick Strex S device with dual gears and **b**, with single gear. Both of the devices can be easily combined to cell culture and images show the cell culture well attached to the membrane. **c**, Side and top views of Brick Strex L device and image of the device when a larger cell culture well has been attached to the membrane. **d**, Brick Strex L device base, together with the device itself and the lid attached.

Figure 2. Manual cell stretching and compression experiment with Brick Strex S.

Epithelial cell monolayers were grown on silicon membranes and subjected to stretching or compression in Brick Strex S device. **a**, Epithelial stretching experiment, where epithelium is subjected to 25 % strain. **b**, Cell were stained with DAPI to highlight the nuclei and

immunolabelled against β-catenin. Mechanical straining induced more pronounced nuclear localization of β-catenin in comparison to control samples. **c**, Epithelial lateral compression experiment. **d**, Cells were stained with DAPI to highlight the nuclei and with phalloidin to label the filamentous actin cytoskeleton. Lateral compression led into higher cell density. **e**, Quantification of the cell density after compression. **f**, Similar lateral compression experiments as in c. Here, the cells were stained with DAPI to highlight the nuclei and immunolabeled against YAP1, which more pronounced localization to cell membrane is visible. **g**, Similar lateral compression experiments as in c. The cells were stained with DAPI to highlight the nuclei and immunolabeled against β-catenin. Lateral compression induced clear accumulation of β-catenin to the cell-cell junctions, as seen in the blowup images. Scale bars 10 μm.

Figure 3. Western blot analysis of lateral compression -induced effects on β-catenin and YAP1. Epithelial cells were cultured on prestrained Si-membrane in Brick Strex S device until full confluency. Following sequential membrane relaxation and increased lateral compression, cells were let to recover for 2 h prior to cell lysis and analyzed by western blot (n=2). **a**, Expression and phosphorylation (S127P) status of YAP1 and **b,** expression of β-catenin were analyzed from whole cell lysates of non-compressed (before) and compressed (after) samples (20 μg of total protein per sample). The analysis showed increased YAP1 cleavage but equal S127 phosphorylation in response to compression in comparison to the non-manipulated controls. In concert, compression lead to increased presence of full-length (FL) and higher molecular weight β-catenin. Arrows indicate the compression-induced cleavage products of YAP1. Asterisk indicates the presence of full-length (FL) and higher molecular weight β-catenin in the compressed sample. β-actin was used as an internal control.

Figure 4. Live-cell compression studies with Brick Strex L.

Epithelial cell monolayers were grown on prestrained silicon membranes and subjected to lateral compression in Brick Strex L device mounted on inverted microscope. **a**, Scheme of the manual relaxation experiment. Cells are grown on prestrained membrane, the membrane is relaxed in approximately 25 cycles of relaxation and imaging, and the data is then processed. **b**, Epithelial cells expressing nuclear lamin A chromobody show packing of the nuclei during the relaxation steps. **c**, Motorization of the Brick Strex L device was achieved with LEGO® EV3 Intelligent Brick, motor M and color sensor (see also Supplementary Figure 5), allowing the motorized system to be mounted on a microscope. The motor performance was measured

by measuring the time for one full cycle of movement. The strain velocity, measured as strain-% / s, is highly linear function of the motor speed setting. **d**, Scheme for the automated cyclic relaxation – stretching experiment. Cells are grown on prestrained membrane, the membrane is subjected to eight relaxation – stretching cycles, imaged and data processed. **e**, Cyclic relaxation cycles show nuclei packing visualized with epithelial cells expressing histone H2B-mCherry fusion protein. Scale bars 50 μm.

Figures

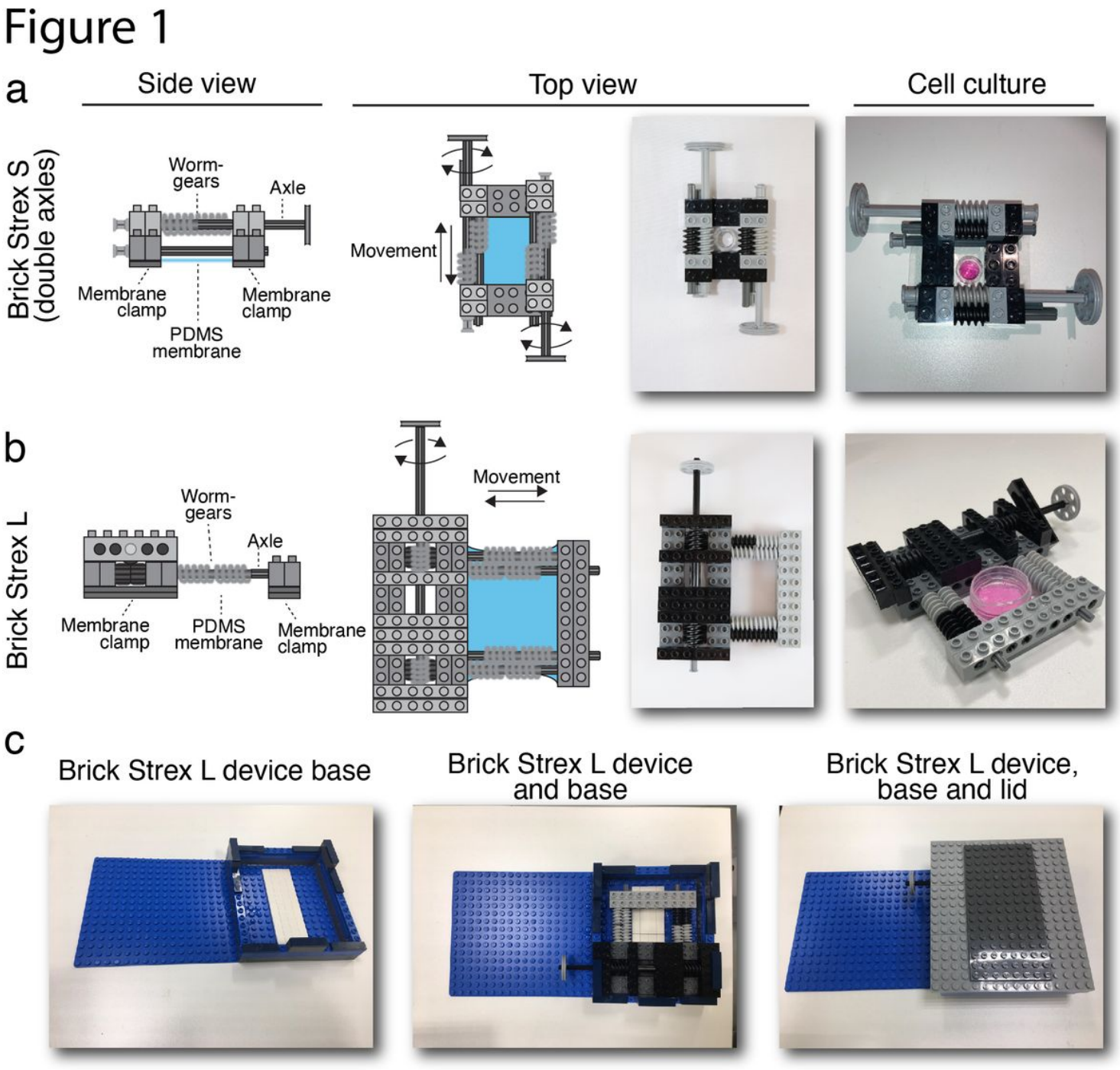

Figure 1

Brick Strex devices and their structure. Design of the various cell stretching devices built of LEGO® bricks. a, Side and top views of Brick Strex S device with dual gears and b, with single gear. Both of the devices can be easily combined to cell culture and images show the cell culture well attached to the membrane. c, Side and top views of Brick Strex L device and image of the device when a larger cell culture well has been attached to the membrane. d, Brick Strex L device base, together with the device itself and the lid attached.

Figure 2

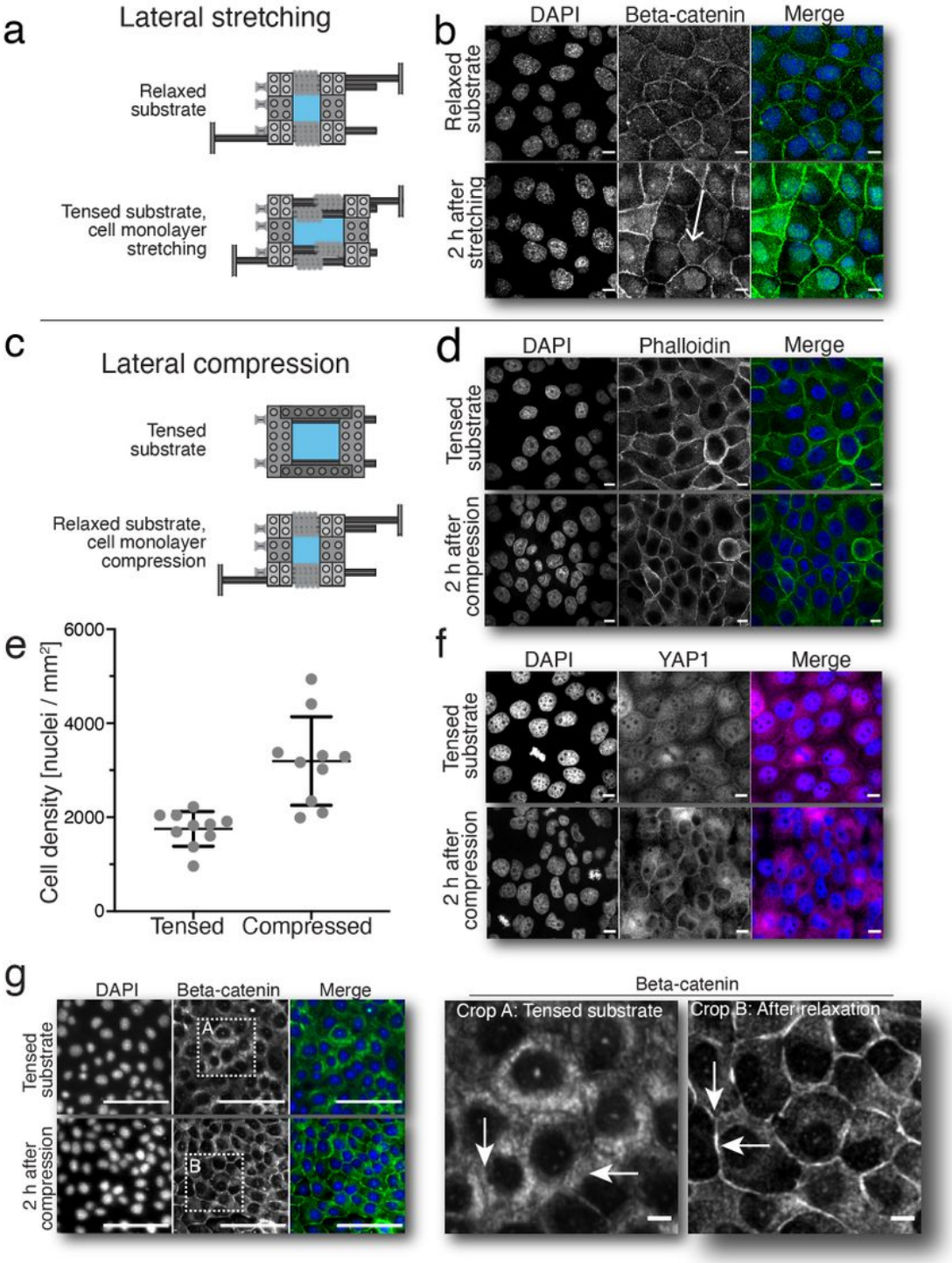

Figure 2

please see the manuscript file for the full caption

Figure 3

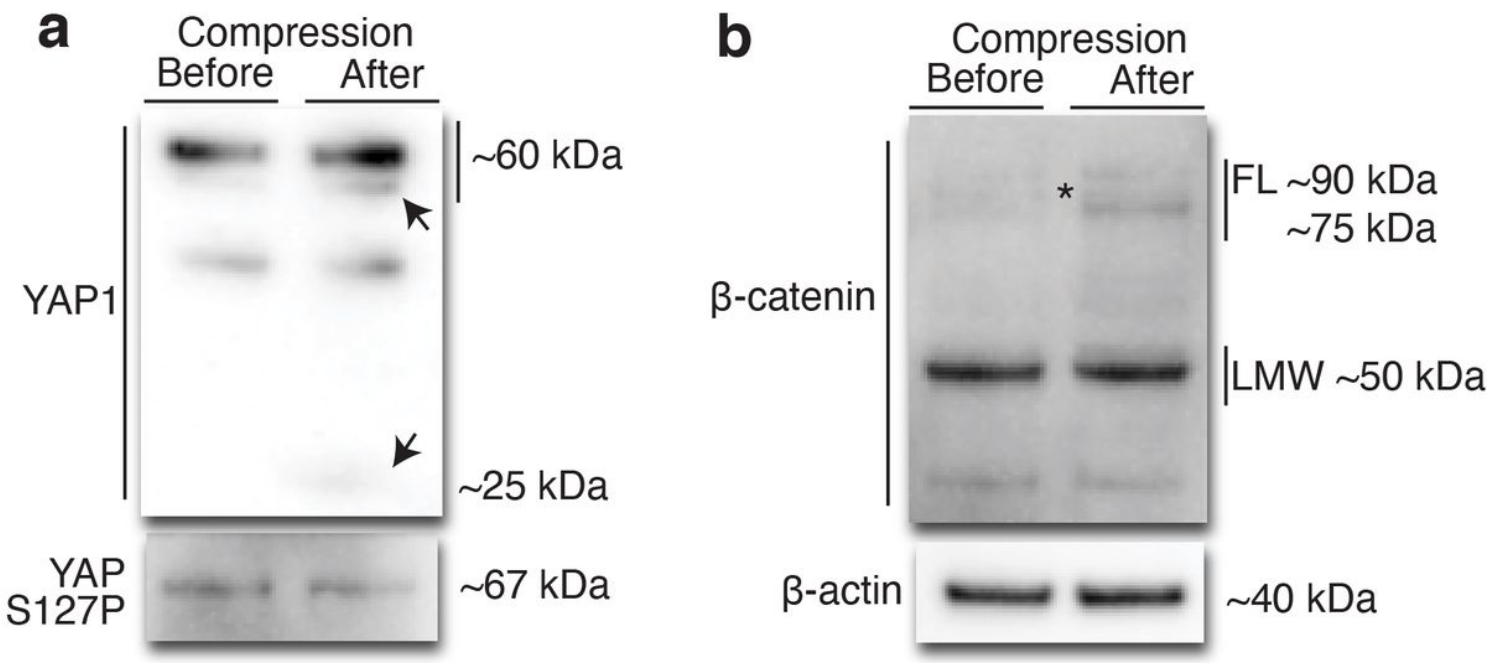

Figure 3

please see the manuscript file for the full caption

Figure 4

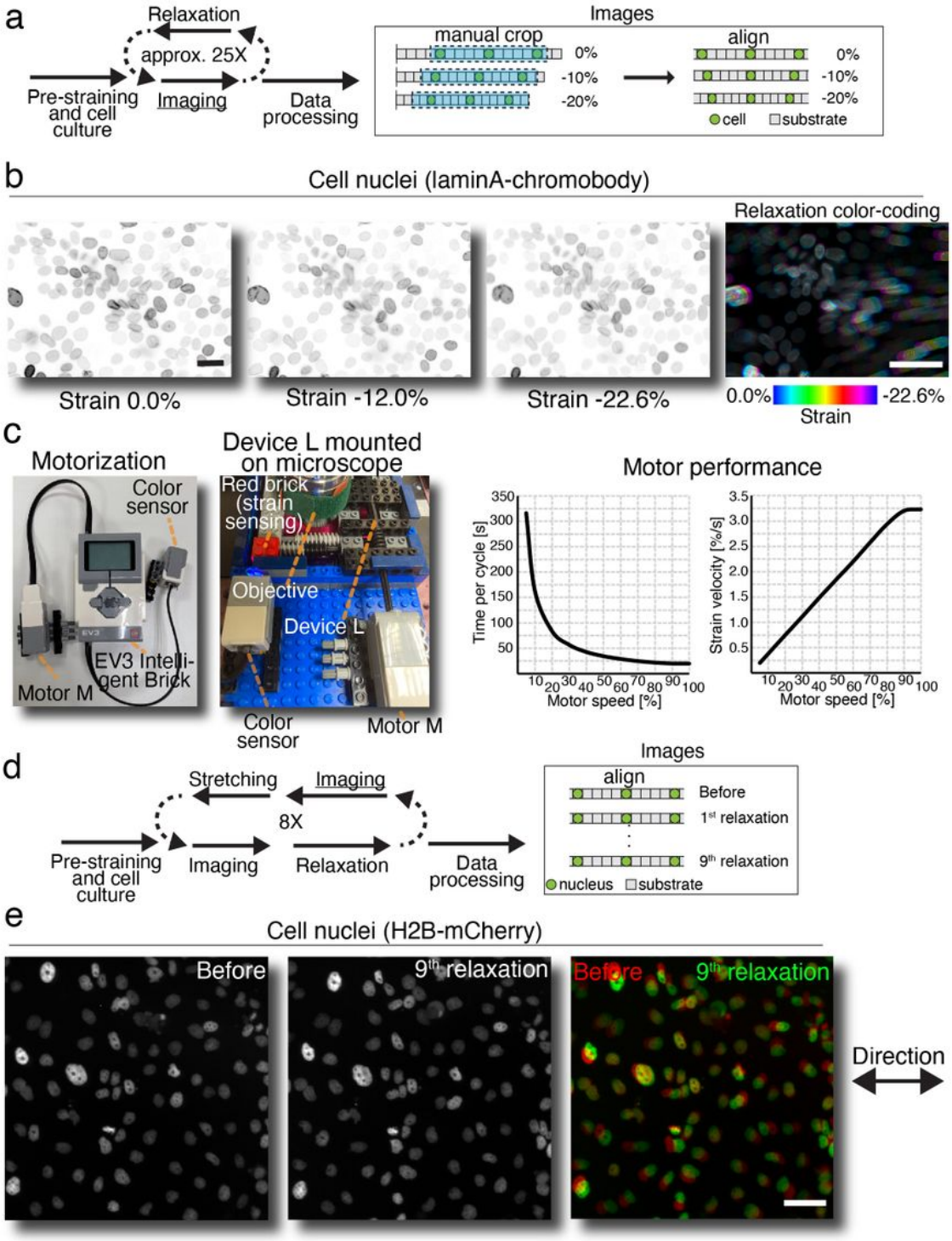

Figure 4

Live-cell compression studies with Brick Strex L. Epithelial cell monolayers were grown on prestrained silicon membranes and subjected to lateral compression in Brick Strex L device mounted on inverted microscope. a, Scheme of the manual relaxation experiment. Cells are grown on prestrained membrane, the membrane is relaxed in approximately 25 cycles of relaxation and imaging, and the data is then processed. b, Epithelial cells expressing nuclear lamin A chromobody show packing of the nuclei during

the relaxation steps. c, Motorization of the Brick Strex L device was achieved with LEGO® EV3 Intelligent Brick, motor M and color sensor (see also Supplementary Figure 5), allowing the motorized system to be mounted on a microscope. The motor performance was measured by measuring the time for one full cycle of movement. The strain velocity, measured as strain-% / s, is highly linear function of the motor speed setting. d, Scheme for the automated cyclic relaxation – stretching experiment. Cells are grown on prestrained membrane, the membrane is subjected to eight relaxation – stretching cycles, imaged and data processed. e, Cyclic relaxation cycles show nuclei packing visualized with epithelial cells expressing histone H2B-mCherry fusion protein. Scale bars 50 µm.

Supplementary Files

This is a list of supplementary files associated with this preprint. Click to download.

- Supplementarymaterial.docx
- Supplementarymovie1.mp4
- Supplementarymovie2.mp4
- Suplementarymovie3.mp4